JACS
JOURNAL OF THE AMERICAN CHEMICAL SOCIETY
pubs.acs.org/JACS
Article

Biosynthesis of 4-Acyl-5-aminoimidazole Alkaloids Featuring a New Friedel−Crafts Acyltransferase

Yuwei Xia,[⊥] Guoliang Zhu,[⊥] Xingwang Zhang,[⊥] Shengying Li, Lei Du,* and Weiming Zhu*

Cite This: https://doi.org/10.1021/jacs.3c09522
Read Online

ABSTRACT: Friedel−Crafts acylation (FCA) is a highly beneficial approach in organic chemistry for creating the important C−C bonds that are necessary for building intricate frameworks between aromatic substrates and an acyl group. However, there are few reports about enzyme catalyzed FCA reactions. In this study, 4-acyl-5-aminoimidazole alkaloids (AAIAs), streptimidazoles A−C (**1**−**3**), and the enantiopure (+)-nocarimidazole C (**4**) as well as their ribosides, streptimidazolesides A−D (**5**−**8**), were identified from the fermentation broth of *Streptomyces* sp. OUCMDZ-944 or heterologous *S. coelicolor* M1154 mutant. The biosynthetic gene cluster (*smz*) was identified, and the biosynthetic pathway of AAIAs was elucidated for the first time. *In vivo* and *in vitro* studies proved the catalytic activity of the four essential genes *smzB*, *-C*, *-E*, and *-F* for AAIAs biosynthesis and clarified the biosynthetic process of the alkaloids. The ligase SmzE activates fatty acyl groups and connects them to the acyl carrier protein (ACP) holo-SmzF. Then, the acyl group is transferred onto the key residue Cys49 of SmzB, a new Friedel−Crafts acyltransferase (FCase). Subsequently, the FCA reaction between the acyl groups and 5-aminoimidazole ribonucleotide (AIR) occurs to generate the key intermediate AAIA-nucleotides catalyzed by SmzB. Finally, the hydrolase SmzC catalyzes the *N*-glycosidic bond cleavage of the intermediates to form AAIAs. Structural simulation, molecular modeling, and mutational analysis of SmzB showed that Tyr26, Cys49, and Tyr93 are the key catalytic residues in the C−C bond formation of the acyl chain of AAIAs, providing mechanistic insights into the enzymatic FCA reaction.

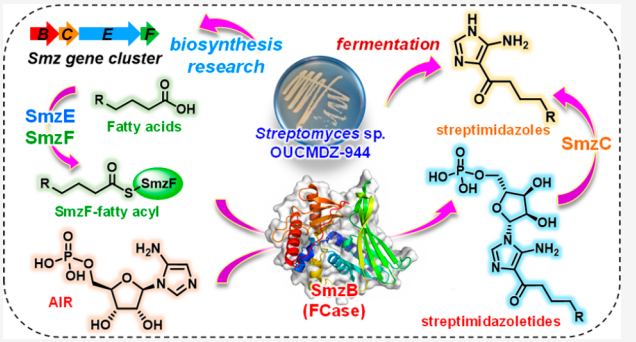

INTRODUCTION

Friedel−Crafts acylation (FCA) is an important reaction in organic chemistry used to form C−C bonds between aromatic substrates and an acyl group, and the formation of C−C bonds is the critical step in the construction of compound skeletons.[1,2] In organic synthesis, such reactions are carried out using an acyl halide or anhydride in the presence of a Lewis acid.[1−3] Although the chemical FCA reaction avoids side reactions such as rearrangement and polyalkylation in Friedel−Crafts alkylation, the FCA reaction still does not occur in aromatic substrates with strong deactivating rings such as nitrobenzene, and aromatic amines are considered as poor substrates because the acylation will preferentially take place on these unprotected amine groups instead of the aromatic ring.[2,4,5] Moreover, there are few reports about enzyme-mediated FCA reactions.[6,7] Therefore, it is a valuable to discover new biocatalysts that can catalyze the FCA reaction.

In recent years, the development of enzyme catalysis has been in full swing, but there are still a few studies on the Friedel−Crafts acyltransferase (FCase) due to its rarity. The 2,4-diacetylphloroglucinol (DAPG) acetyltransferase (ATase), which is encoded by genes *phlABC* in the biosynthetic gene cluster (BGC) of the polyketide antibiotic DAPG, is currently the only kind of FCase discovered.[8,9] Based on the study of crystal structure and catalytic mechanism, the DAPG ATase (*Pp*ATaseCH) from the strain *Pseudomonas protegens* DSM 19095 was rationally engineered to expand its acyl donor substrate scope.[10−15] However, the *Pp*ATaseCH is only able to catalyze aromatic substrates of benzene-1,3-diol and its derivatives, which exposes its great limitations on aromatic substrates.[10] The discovery of new FCases that can catalyze different types of aromatic substrates is crucial for the further development of FCase-like biocatalysts.

4-Acyl-5-aminoimidazole alkaloids (AAIAs), bearing a 5-aminoimidazole ring and a conjugated carbonyl side chain, represent a kind of rare natural products of microbial origin.[16] To date, only four AAIAs, nocarimidazoles A−D, have been reported from marine actinomycetes.[16,17] To discover interesting alkaloids from microorganisms, we examined strain *Streptomyces* sp. OUCMDZ-944 that was isolated from a

Received: August 31, 2023
Revised: October 21, 2023
Accepted: November 6, 2023

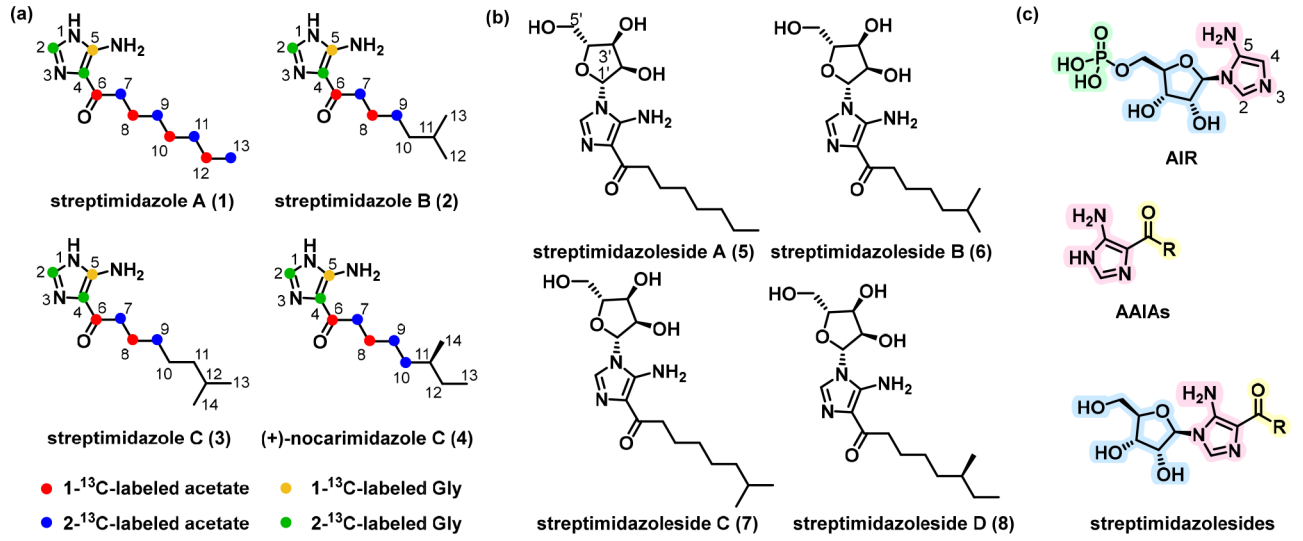

Figure 1. Structures of compounds **1**−**8** and AIR. (a) Use of ^{13}C-labeled precursors for tracking the source of carbons in **1**−**4**. (b) Structures of compounds **5**−**8**. (c) Structural correlation between AIR, AAIAs, and streptimidazolesides.

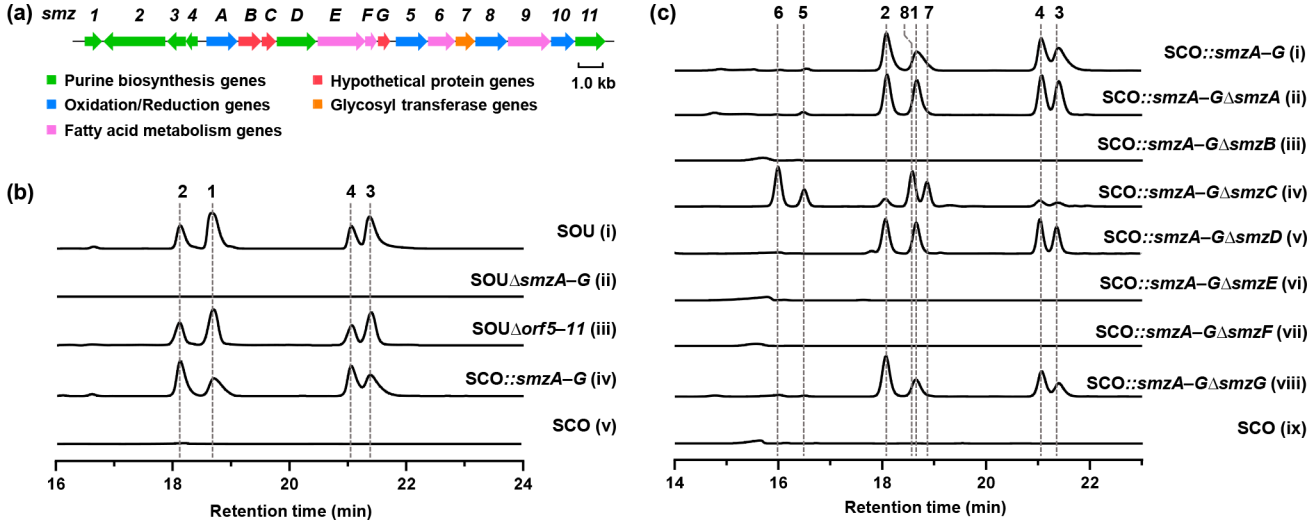

Figure 2. *In vivo* functional analysis of AAIAs biosynthetic genes. (a) AAIAs biosynthetic gene cluster (*smz*). (b) HPLC analysis of *Streptomyces* sp. OUCMDZ-944 (SOU) and *S. coelicolor* M1154 (SCO) with *smzA*−*G* expressed. (c) HPLC analysis of strain SCO::*smzA*−*G* and its single gene deletion mutants.

sediment sample collected off the coast of Qingdao, China. Fractionations of its metabolites led to the discovery of seven new AAIAs, including streptimidazoles A−C (**1**−**3**) and streptimidazolesides A and B (AAIA-1-ribosides, **5** and **6**), as well as the enantiopure (+)-nocarimidazole C (**4**) (Figure 1a,b).[17] Besides, two new AAIA-1-ribosides, streptimidazolesides C (**7**) and D (**8**), were identified from the metabolites of the heterologous *S. coelicolor* M1154::*smzA*−*G*Δ*smzC* (Figure 1b). The conjecture of the origin of the AAIAs and further verification from the ^{13}C labeling experiment led us to propose the hypothesis that the 5-aminoimidazole ring and alkanoyl moiety of these alkaloids are derived from the 5-aminoimidazole-1-ribotide (AIR) in purine biosynthesis and fatty acids synthesized by acetic acid−malonic acid (AA-MA) pathway, respectively. The identification of streptimidazolesides **5**−**8** has strengthened our confidence in this conjecture.

To date, there are no reports on the biosynthesis of AAIAs. Research on the biosynthetic pathway seems to be challenging, interesting, and valuable, as it does not belong to any typical secondary metabolic routes based on the analysis of the chemical structure. On the contrary, it is closely related to the primary metabolism, which may lead to a deeper understanding of the cross-talk between primary metabolism and secondary metabolism. At the same time, it raises the question of how the C−C bonds between the C-4 in 5-aminoimidazole ring of AIR and acyl carbon in the alkanoyl moiety are formed, which is the key step in the biosynthesis process of AAIAs. The exploration of the corresponding enzyme responsible for this biocatalytic reaction may lead us to discover a new FCase.

Under the guidance of bioinformatics analysis, we successfully identified the biosynthesis gene cluster (*smz*) (Figure 2a) of AAIAs from 42 gene clusters predicted by antiSMASH (version 5.0.0)[18] through gene knockout and heterologous expression experiments. *In vivo* and *in vitro* assays proved that four essential genes *smzB*, *-C*, *-E*, and *-F* catalyzed the biosynthetic assembly of AAIAs from the precursors AIR and fatty acids. It is the first case that AIR is found to be a building block in natural product biosynthesis. SmzB is

https://doi.org/10.1021/jacs.3c09522
J. Am. Chem. Soc. XXXX, XXX, XXX−XXX

revealed as a new FCase to catalyze the FCA reaction between the acyl groups and AIR, generating the key intermediate streptimidazoletides A−D (AAIA-1-ribotides, **9**−**12**). The further mechanism elucidation and phylogenetic analysis of SmzB expand the understanding of the new FCase family. The successful elucidation of the phylogenetic pathway of the AAIAs provides effective ideas and guidance for the study of the biosynthesis of such alkanoylimidazole alkaloids.

RESULTS AND DISCUSSION

Discovery of Streptimidazoles and Riboside Derivatives. Analysis of the ethyl acetate (EtOAc) extract of *Streptomyces* sp. OUCMDZ-944 showed that there are a series of metabolites with characteristic UV absorptions around λ_{max} = 300 nm. Further analysis by liquid chromatography−mass spectrometry (LC−MS) revealed four predominant compounds and four trace additional compounds with the molecular weights of 209, 209, 223, 223, 341, 341, 355, and 355 Da, respectively (Figure S15). The consistent mass difference of 14 Da suggests a structural relationship between them, which is homologous compounds. Through large-scale fermentation, five new compounds, including streptimidazoles A−C (**1**−**3**) and two of their trace ribosides streptimidazolesides A and B (**5** and **6**), as well as the enantiopure congener, (+)-nocarimidazole C (**4**), were identified (Figure 1a,b). In the process of structural analysis of these alkaloids, we found that the ^{13}C signals at positions C-2, C-4, C-5, and C-6 of **1**−**4** were low, broadened, and barely visible (Figure S2). Chemically, this could be attributed to the tautomerism of the 5-aminoimidazole ring between N and NH.[16] To verify these structures, **1** was taken as an example to perform methylation experiments. A pair of monomethyl derivatives **13** (at *N*-1 position) and **14** (at *N*-3 position) were obtained by fine control of the reaction conditions involving the incubation time, the base type (NaH or Na_2CO_3), and the amount of CH_3I (Figure S1a). As expected, the ^{13}C signals of the two methylated products returned to normal (Figure S1b), and the NMR (Figure S1a and Table S9) matched well with the predicted structures, confirming the structural accuracy of **1**−**4**. Meanwhile, the ^{13}C signals at these positions of **5** and **6** are comparable to those of **13** (Figure S7), indicating there are substitutions at the *N*-1 position of the 5-aminoimidazole ring. The substitution group in **5** and **6** was further identified to be the D-ribose by comprehensive analysis of 1D and 2D NMR (Figures S4 and S5), hydrolysis of **5** followed by 1-phenyl-3-methyl-5-pyrazolone (PMP) derivation (Figure S4), and electronic circular dichroism (ECD) data (Figure S5). Therefore, compounds **5** and **6** were D-ribosides of **1** and **2**, respectively.

Inference of Biosynthesis Pathway by Isotope Labeling Experiments. Considering that the 5-aminoimidazole ring of AAIAs and the glycosidic 5-aminoimidazole substructure of streptimidazolesides share high structural similarity with AIR, a key intermediate of purine biosynthesis, we reasoned that AIR might be the precursor of such alkaloids (Figure 1c).[19] To verify this, we performed isotope feeding assays with ^{13}C-labeled glycine, as glycine is one of the precursors for the synthesis of AIR (Figure S6c).[20,21] Meanwhile, the feeding experiments of ^{13}C-labeled acetate were also carried out based on the conjecture that the carbonyl side chain was formed by the AA-MA pathway (Figure S10).

To clearly observe the ^{13}C signal gain at C-2, C-4, C-5, and C-6, 1-^{13}C acetate-feeding product (**1a**) and 1- and 2-^{13}C glycine-feeding products (**1d** and **1e**) of streptimidazole A (**1**) were methylated to obtained 1-methylated derivatives (**13a**, **13b**, and **13c**). As expected, in the 5-aminoimidazole ring, the carbon signal of C-5 in **13b** (feeding 1-^{13}C-labeled glycine) and the C-2 and C-4 carbon signals in **13c** (feeding 2-^{13}C-labeled glycine) were significantly enhanced (Figures 1a and S6b). The carbon signals of C-6, C-8, C-10, and C-12 in **13a** (feeding 1-^{13}C-labeled acetate) also showed a significant enhancement compared to the unlabeled methylated product **13** (Figures 1a and S6a). For the carbonyl side chain of **1b** (feeding 2-^{13}C-labeled acetate), ^{13}C signal enhancements occur at odd-number carbons (C-7, C-9, C-11, and C-13) (Figures 1a and S8). And the feeding 1,2-^{13}C-labeled acetate led to a significant enhancement of carbon signals for C-6−C-13 in **1c** (Figures 1a and S8).

For the carbonyl side chains of **2**−**4**, ^{13}C signal enhancements occur at C-6 and C-8 when fed with 1-^{13}C-acetate and at C-7 and C-9 when fed with 2-^{13}C-acetate (Figures 1a, S8, and S9). These results are quite consistent with the rule of carbon chain extension in fatty acid synthesis (Figure S10).[22,23] In addition, C-10−C-13 in **2**, C-10−C-14 in **3**, and C-11−C-14 in **4** did not show the ^{13}C signals enhancement (Figures 1a, S8, and S9), indicating that the fatty acids used to synthesize AAIAs have different start units before carbon chain extension. These starting carbon atoms are considered to come from the metabolic pathways of valine, leucine, and isoleucine (Figure S10).[24−26] This inference also explains why the ^{13}C signal of C-10 in **4** was also enhanced when feeding 2-^{13}C-labeled acetate, as acetyl-coenzyme A (acetyl-CoA) is one of the raw materials for the synthesis of isoleucine (Figures S9 and S10).[27] These results strongly suggest that AAIAs are biosynthesized using precursors AIR and fatty acids from primary metabolism.

Identification and Characterization of AAIAs Biosynthetic Genes. The biogenesis analysis of AAIAs provided important information for us to speculate on the biosynthetic pathway and identify the BGC. It also suggested that the most critical step in the biosynthesis is the C−C bond formation between C-4 of AIR and C-1 of fatty acids via the proposed FCA reaction. To identify the AAIAs BGC and characterize the putative key FCase, the genome of the strain OUCMDZ-944 was sequenced and analyzed by antiSMASH.[18] A gene cluster (*smz*) rich in genes related to the purine biosynthesis seemed to be the most likely BGC for AAIAs (Figure 2a and Table S4). Bioinformatics analysis showed that genes *orf1* (*purN*), *orf2*−*4* (*purL*, *purQ*, and *purS*) and *orf11* (*purM*) in this BGC are associated with converting glycinamide ribonucleotide (GAR) into AIR (Figure S6c and Table S4), and all of them have homologous genes (77−100% in identity) in other locations of the genome (Table S5).[19,28−30] Knockout of the genes *orf2* and *orf3* resulted in a certain reduction in the yield of compounds **1**−**4** (Figure S16), which shows that the existence of these gene copies in the BGC plays a significant role in providing sufficient AIR for biosynthesis of AAIAs.

On this basis, we further analyzed the function of the genes in *smz* BGC (Table S4) and found that three genes *smzB*, *smzC*, and *smzG* encode hypothetical proteins, one of which is most likely to encode the new FCase we are looking for. In view of the distribution and sequence correlation of adjacent genes in the BGC, we reason that genes *smzA*−*G* and *orf5*−*11* belong to two individual transcriptional units. To locate the necessary genes required for AAIAs biosynthesis, large fragment knockouts toward the two transcriptional units

https://doi.org/10.1021/jacs.3c09522
J. Am. Chem. Soc. XXXX, XXX, XXX−XXX

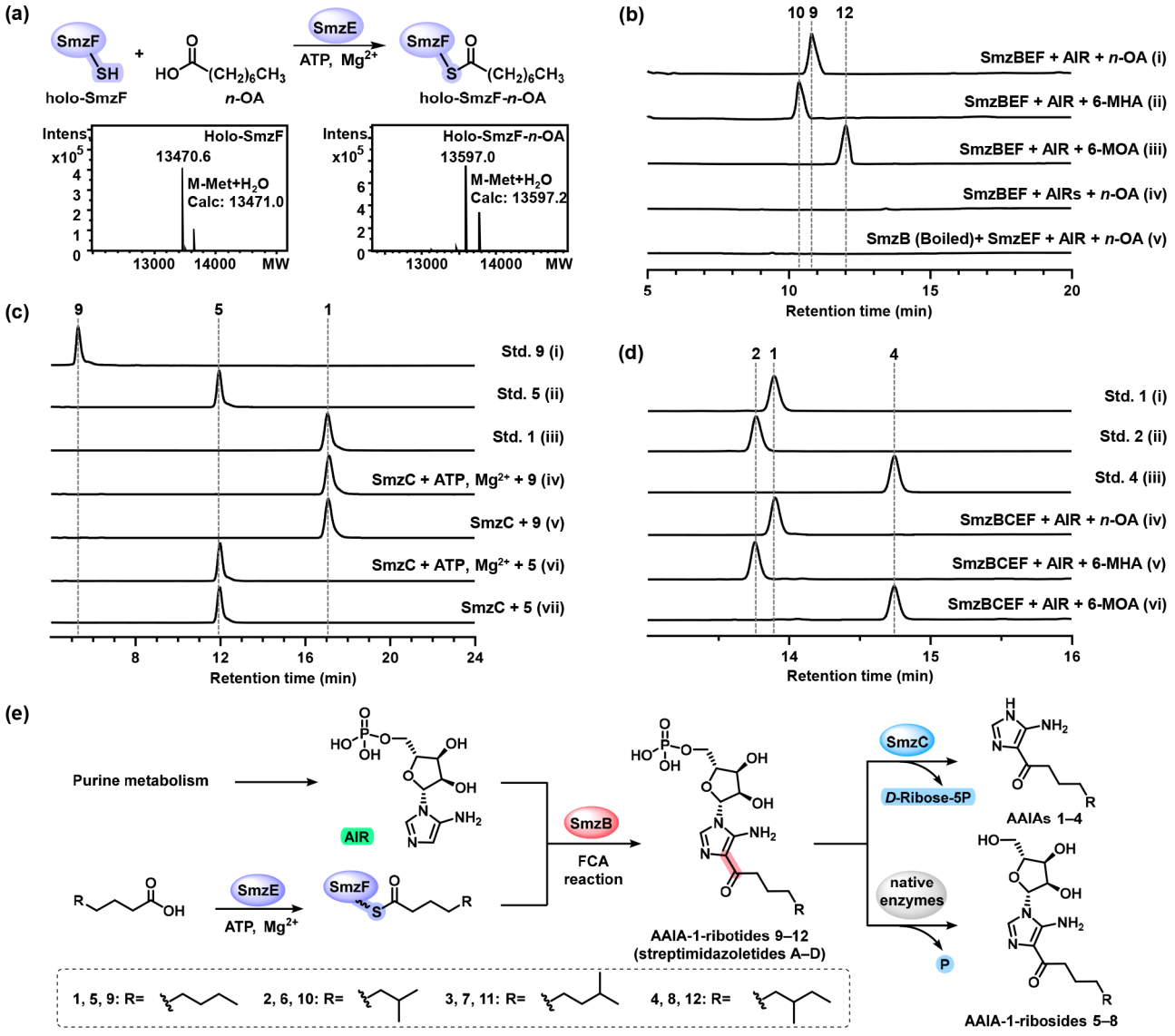

Figure 3. *In vitro* functional elucidation of AAIAs biosynthetic genes. (a) ESI-Q-TOF-MS analysis of SmzE and SmzF reaction. (b) HPLC analysis of coupling enzymatic reactions of SmzB, SmzE, and SmzF with AIR (5-aminoimidazole-1-ribotide) or AIRs (5-aminoimidazole-1-riboside) and fatty acids. (c) HPLC analysis of SmzC reactions. (d) HPLC analysis of coupling enzymatic reactions of SmzB, SmzC, SmzE, and SmzF. (e) Biosynthetic pathway of AAIAs.

were performed (Figure S17). As a result, the strain with genes *smzA*−*G* knocking out no longer produced AAIAs (Figure 2b, trace ii, while that with *orf5*−*11* mutated exhibited the similar phenotype as the wild-type one (Figure 2b, trace iii). These results strongly indicated that the genes necessary for the biosynthesis of AAIAs are all among *smzA*−*G*. To ensure this, these genes were heterologously coexpressed in *S. coelicolor* M1154 under the strong promoter kasOp*.[31] As expected, the strain with genes *smzA*−*G* inserted into the genome successfully produced AAIAs (Figure 2b, trace iv), and the yield of compounds **1**−**4** is much lower than the WT strain *Streptomyces* sp. OUCMDZ-944, suggesting the important role of the additional purine biosynthesis genes in the *smz* cluster (Figure S16b).

To characterize the function of each gene, we further constructed seven individual single-gene knockout mutants based on the strain *S. coelicolor* M1154::*smzA*−*G* (Figure S18). Secondary metabolites analysis of these mutants showed that the deletion of *smzB*, *smzE*, and *smzF*, completely blocked the production of AAIAs (Figure 2c traces iii, vi, and vii), and the absence of gene *smzC* led to the accumulation of streptimidazolesides A−D (**5**−**8**) as well as the trace amounts of **1**−**4** (Figure 2c, trace iv), while knockout other genes (*smzA*, *smzD*, or *smzG*) had no effect on the fermentation profile (Figure 2c, traces ii, v, and viii). Compounds **5** and **6** have been previously isolated and characterized. Based on NMR and ECD data (Figures S4 and S5), we identified **7** and **8**, which were isolated from the EtOAc extract of the *smzC* mutant strain, as the ribosides of **3** and **4** (Figures 1b, S4, and S5).

The above fermentation and the product analysis of the single gene knockout strains revealed that genes *smzB*, *smzC*, *smzE*, and *smzF* are necessary for the biosynthesis of the AAIAs skeletons. The accumulation of ribosides **5**−**8** indicates that they may be the catalytic products of SmzB, SmzE and SmzF and may also be the substrates of SmzC (Figure 2c, trace iv). Combined with the above results and the predicted protein functions (Table S4), SmzB is most likely to be the key FCase,

https://doi.org/10.1021/jacs.3c09522
J. Am. Chem. Soc. XXXX, XXX, XXX−XXX

and the biosynthesis of AAIAs can therefore be deduced as follows: Protein SmzB catalyzes the FCA reaction between AIR and fatty acids, which are initially activated and linked to acyl carrier protein (ACP) SmzF by the ligase SmzE, and then SmzC causes the cleavage of *N*-glycosidic bonds to produce AAIAs.

Functional Elucidation of SmzB, SmzC, SmzE, and SmzF. To further clarify the catalytic function of the genes *smzB*, *smzC*, *smzE*, and *smzF*, *in vitro* enzymatic assays were further carried out. The four proteins were expressed in *Escherichia coli* BL21 (DE3) and purified (Figure S19). The *smzE* and *smzF* genes are predicted to encode fatty acid-AMP ligase and ACP (Table S4), indicating they are responsible for activating fatty acids. In order to directly obtain the active holo-SmzF, the ACP SmzF was coexpressed with protein surfactin phosphopantetheinyl transferase (Sfp from *Bacillus subtilis*).[32,33] Electrospray ionization-quadrupole-time-of-flight-mass spectrometry (ESI-Q-TOF-MS) analysis revealed that the calculated protein molecular weight (MW) of Sfp-activated holo-SmzF increased 340 Da compared with apo-SmzF expressed alone (Figures S20a and S21a,b), indicating that the 4′-phosphopantetheine moiety of CoA was successfully covalently linked to the putative conserved serine residue of SmzF. Subsequently, *n*-octanoic acid (*n*-OA), which is predicted to be the precursor of the fatty acyl side chain in **1**, was used as a substrate to verify the catalytic function of SmzE and SmzF. As expected, in the presence of cosubstrate ATP and cofactor Mg^{2+}, the observed MW of protein product was increased by 126 Da as evidenced by the positive ESI-Q-TOF-MS analysis, proving that *n*-OA was catalytically activated by SmzE and loaded into the putative sulfhydryl grip of holo-SmzF (Figures 3a, S20b,c, and S21b−e). As AAIAs showed structural diversity in the fatty acyl side chains, we speculated that 6-methylheptanoic acid (6-MHA), 7-methyloctanoic acid (7-MOA), and 6-methyloctanoic acid (6-MOA) are precursors of compounds **2**−**4**, respectively. In addition to *n*-OA, we have also tested other two commercially available fatty acids (6-MHA and 6-MOA), both of which can also be effectively linked to holo-SmzF (Figures S20d,e and S21f,g).

After verifying the functions and reaction conditions of SmzE and SmzF, we then investigated the function of SmzB. Using a chemoenzymatic approach (see Supporting Information methods), we successfully synthesized the key precursor AIR which was predicted to be the source of the 5-aminoimidazole ring in AAIAs. We then carried out enzyme coupling reactions of SmzB, SmzE, and SmzF, using AIR and *n*-OA as substrates under the conditions of ATP and Mg^{2+}. The results of HPLC and LC−high-resolution MS (LC−HRMS) analyses clearly showed that a new compound **9** with a MW of 421 Da was generated (Figures 3b, trace i, S22, and S23). The 80 Da difference in MW between the product **9** and the riboside **5** suggested that the product **9** might be the 5′-monophosphorylate of **5**, considering the structural characteristic of AIR. When *n*-OA was replaced by the other two fatty acids, 6-MHA and 6-MOA, products **10** and **12** were formed with MWs of 421 and 435, respectively (Figures 3b, traces ii and iii, S22, and S23). We also searched the extracted ion chromatogram (EIC) at *m*/*z* 422 and 436 $[M + H]^+$ (corresponding to compounds **9**−**12**) from the LC−HRMS data for the metabolites of the SmzB, SmzE, and SmzF coexpressed strain *S. coelicolor* M1154::*smzA*−*G*Δ*smzC*. Results showed that four peaks (**9**−**12**) were found and three of them are consistent with the available products of the enzyme coupling reactions of SmzB, SmzE, and SmzF (Figures S22 and S24). To further determine the structures of **9**−**12**, we chemically synthesized the hypothetical structures by phosphorylation of ribosides **5**−**8** using triethyl phosphate (TEP) and $POCl_3$ (see Supporting Information methods). Co-HPLC analysis with the synthetic standards confirmed the structures of **9**−**12** as the AAIA-1-ribotides, namely, streptimidazoletides A−D (Figures 3c and S27). These results strongly demonstrated that SmzB catalyzes the formation of **9**−**12** from AIR and the active fatty acids.

Cascade reactions of SmzB, SmzE, and SmzF only generated AAIA-1-ribosidyl-5′-phosphates, that is, AAIA-1-ribotides. However, the three genes coexpressed strain *S. coelicolor* M1154::*smzA*−*G*Δ*smzC* mainly produced nonphosphorylated **5**−**8** in addition to a small amount of **1**−**4** and the negligible amount of **9**−**12** (Figures 2c, trace iv, and S24). Considering these differences in product distribution and chemical structure between *in vitro* and *in vivo* assays, we further investigated whether the 5-aminoimidazole-1-riboside (AIRs) could be used directly as a substrate for this gene to catalyze the production of nonphosphorylated products. HPLC analysis showed that no products were generated (Figure 3b, trace iv), indicating that the nonphosphorylated AIRs cannot be directly recognized by SmzB. These findings suggest that 5′-nonphosphorylated products **5**−**8** are generated after 5′-phosphoylated compounds **9**−**12** in the strain *S. coelicolor* M1154::*smzA*−*G*Δ*smzC*. We speculate that the catalytic products **9**−**12** of SmzB may be hydrolyzed by native enzymes such as 5′-monophosphate phosphohydrolase to form **5**−**8** or undergo a phosphoribosyl transfer reaction by phosphoribosyltransferase to generate **1**−**4**, based on their structural similarity with ribotides.[34,35] And this is supported by feeding experiments that **9** or **5** was added into wild-type *S. coelicolor* M1154 under the same fermentation conditions. HPLC analysis indicated that more than 99% of streptimidazoletide A (**9**) would be metabolized to generate streptimidazoleside A (**5**) (83%) and streptimidazole A (**1**) (16%). Meanwhile around 13% of **5** could be converted into **1**, and their relative abundance was qualitatively consistent with the observation in *smzC* mutant strain (Figures 2c, trace iv, and S25).

The protein SmzC showed some similarities (41.9% protein identity) to the nucleoside 2-deoxyribosyltransferase (Table S4). To investigate the real substrate of SmzC and determine whether ATP and Mg^{2+} are necessary for its activity, enzymatic assays with compounds **9** and **5** were subsequently carried out. HPLC analysis showed that the substrate **9** instead of **5** could be transformed into corresponding product **1**, whether or not ATP and Mg^{2+} were present in the reaction system (Figure 3c). LC−HRMS analysis further clarified that SmzC catalyzed **9** to produce **1** and D-ribose 5-phosphate by searching *m*/*z* at 208 and 229 $[M - H]^-$ (Figure S26). Meanwhile, we also tested the other phosphates **10**−**12**, all of which could be transformed into the corresponding products **2**−**4** under the catalysis of SmzC (Figure S27). These results demonstrated that AAIA-1-ribotides are the real substrates of SmzC. Moreover, it has been established that SmzC functions as a hydrolase, as opposed to a phosphoribosyltransferase or phosphorylase, since D-ribose 5-phosphate was detected as the co-product during the catalytic reaction.[35−37]

Based on the analysis above, we conducted one-pot enzymatic reactions of SmzB, SmzC, SmzE and SmzF to synthesize AAIAs *in vitro*. As expected, corresponding products **1**, **2**, and **4** were obtained by adding *n*-OA, 6-MHA, and 6-

https://doi.org/10.1021/jacs.3c09522
J. Am. Chem. Soc. XXXX, XXX, XXX−XXX

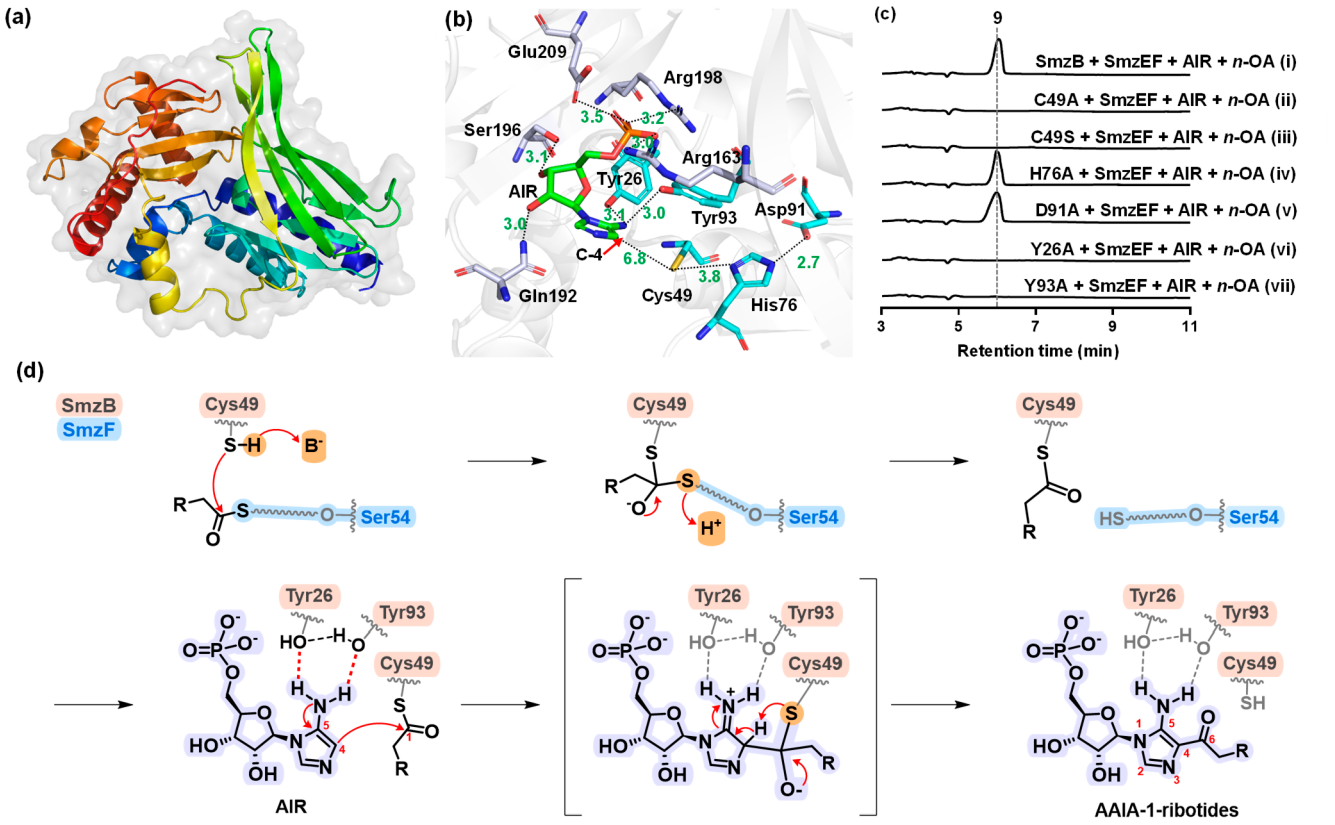

Figure 4. Analysis of the catalytic mechanism of SmzB. (a) Structural overview of SmzB predicted by AlphaFold2. The chain shows in a rainbow color gradient from the N-terminus (blue) to the C-terminus (red). (b) Docked SmzB-AIR complex with the key residues, and hydrogen bonding distances shown in Å. AIR is shown in green. The candidate key residues (Tyr26, Cys49, His76, Asp91, and Tyr93) are shown in blue. Residues that may only be responsible for stabilizing the substrate conformation are shown in blue-white. (c) Site-directed mutagenesis results. (d) The proposed mechanism for the FCA reaction catalyzed by SmzB. SmzB is shown in pink. SmzF and the 4′-phosphopantetheinyl moiety are shown in blue. AIR is shown in purple. The proposed process of proton/electron transfer is shown by red arrows.

MOA to the reaction system (Figure 3d), respectively. Furthermore, we investigated the versatility of the fatty acid substrate by adding linear fatty acids of varying chain lengths ranging from 3C to 16C into the reaction. Remarkably, HPLC analysis showed that the enzyme coupling reaction of SmzB, SmzC, SmzE, and SmzF successfully produces the corresponding AAIAs from linear fatty acids with carbon chain length ranging from 5C to 14C (Figure S28). Among them, seven linear fatty acids (5C−11C) exhibited high yields (73−98%) (Figure S28). However, the corresponding AAIAs were not formed from the one-pot enzymatic reactions when the lengths of linear fatty acids were shorter than 5C or longer than 14C (Figure S28). This could be explained by that these linear fatty acids could not be activated and linked to the ACP holo-SmzF from the protein MS analysis for C4 and C15 fatty acids with SmzF (Figure S29). These results demonstrate that the enzyme reaction system has a wide range of substrate specificity and a robust capacity to synthesize such alkaloid derivatives.

The *in vitro* high yields of analogs with fatty acid moieties have a broad range from 5C to 11C, which is not consistent with the *in vivo* isolated alkaloids with fatty acid moieties of 8C and 9C. We analyzed the EIC at m/z 168 (5C), 182 (6C), 196 (7C), 210 (8C), 224 (9C), 238 (10C), and 252 (11C) $[M + H]^+$ from the LC−MS data for the EtOAc extract of the *Streptomyces* sp. OUCMDZ-944. Besides the main products **1**−**4** (8C and 9C), only trace amounts of the analogs with fatty acid moieties of 6C, 7C, 9C, and 10C were detected in the EtOAc extract (Figure S28c). We speculate that this is probably due to the different concentrations of native fatty acid substrates in the intracellular metabolic environment. This is supported by two pieces of evidence: (i) the production ratio of compounds **1**−**4** produced by SmzBCEF in *Streptomyces* sp. OUCMDZ-944 and heterologous *S. coelicolor* M1154 differed (Figure 2b, traces i and iv), indicating the variation of fatty acid abundance in the strains; (ii) previously reported AAIAs and their analogues have demonstrated a predilection for carbonyl chains of moderate length (C7−C11) for the producing strains.[16,17,38,39]

Thus, the entire biosynthetic pathway of AAIAs has been completely clarified. Under the catalysis of the ligase SmzE, fatty acids are activated and connected to the sulfhydryl group of the ACP holo-SmzF. Next, the FCA reaction occurs between the activated fatty acid and AIR under the catalysis of the FCase SmzB. This subsequently generates the key intermediate AAIA-1-ribotides, which are subjected to the *N*-glycosidic bonds cleavage to form AAIAs catalyzed by the hydrolases SmzC (Figure 3e).

Probing the Catalytic Mechanism of the FCase SmzB.

Based on the results of enzymatic reactions *in vitro* (Figures 3b and S22), protein SmzB was characterized to be the key FCase catalyzing the FCA reaction in AAIAs biosynthesis. To understand the catalytic mechanism, we predicted the 3D structure of SmzB (pLDDT 93.631) using AlphaFold2,[40] which clearly showed a hypothetical catalytic pocket (Figures 4a and S30a). According to the elucidated biosynthetic

https://doi.org/10.1021/jacs.3c09522
J. Am. Chem. Soc. XXXX, XXX, XXX−XXX

pathway of AAIAs, the ACP protein SmzF activates and transfers fatty acids to SmzB. To further explore the interactions between these two proteins, we also performed protein structure prediction for SmzF (Figure S30b). The following docking model and protein−protein interaction (PPI) analysis of SmzB and SmzF showed that SmzF binds to the β-sheet side of SmzB (Figure S30c and Table S7). The conserved serine residue (Ser54) of SmzF, which is supposed to accept the 4′-phosphopantetheinyl moiety of CoA in ACP activation, was identified via multisequence alignment and close to the active pocket of SmzB (Figures S30 and S31). The SmzB-SmzF complex is combined by hydrogen bonds, salt bridges, cation−π stacking, and hydrophobic interactions (Table S7).

After performing a multisequence alignment analysis of SmzB with nine homologous proteins, multiple conserved residue sites were revealed (Figure S32). 40% of these sites, Tyr26, Cys49, His76, Asp91, Tyr93, Arg163, Gln192, Ser196, Arg198, Glu209, and Tyr287, are in the active pocket (Figures S30a and S32). Further conformational analysis of the docking results of SmzB and the substrate AIR as well as product **9** showed that Gln192 and Ser196 have hydrogen bond interactions with the ribose of AIR (Figures 4b and S33). The phosphate group in AIR is stabilized by a plurality of charged residues (Arg163, Arg198, and Glu209) (Figures 4b and S33). Meanwhile, Cys49 faces the key catalytic carbon atom C-4 in AIR (Figures 4b and S33). By analyzing the residues around Cys49, a putative Cys-His-Asp catalytic triad composed of residues Cys49, His76, and Asp91 was discovered (Figure 4b), which has been reported in the structurally similar (TM-score 0.575, RMSDval 3.778) enzyme arylamine *N*-acetyltransferase 2.[41,42] Alignment of SmzB and the arylamine *N*-acetyltransferase 2 showed that their catalytic triads are in consistent spatial positions (Figure S34). Considering the catalytic mechanism of the *N*-acetyltransferases,[42] we speculate that the conserved Cys49 of SmzB should be the acyl receptor for the activated fatty acids transferred by ACP SmzF. The conserved residues Tyr26 and Tyr93 showing interactions with the NH_2 group of the 5-aminoimidazole ring may participate in electron and proton transfer in the FCA catalytic process (Figure 4b).

Based on the above analysis, we propose that the overall catalytic process of SmzB includes the transfer of the fatty acyl from SmzF to Cys49 of SmzB and the formation of C−C bond between the C-4 of AIR and the C-1 of the fatty acyl group. Then, site-directed mutagenesis for the five conserved residues (Tyr26, Cys49, His76, Glu91, and Tyr93) that may be associated with the catalytic process was carried out. Mutant enzymes were expressed in *E. coli* JM109(DE3) and purified to homogeneity (Figure S35). As expected for C49A mutant, the catalytic activity was completely abolished (Figure 4c). And protein MS analysis showed that compared with the wild-type SmzB, the fatty acyl group can no longer be transferred to this mutant protein (Figures S36 and S37). These results clearly demonstrated that Cys49 of SmzB is indeed the fatty acyl receptor. In addition, mutant C49S also lost activity (Figure 4c), indicating the important role of the sulfhydryl group of Cys49 in the reaction. For arylamine *N*-acetyltransferases, the Cys-His-Asp catalytic triad is responsible for the acylation of residue Cys.[42] The residue Asp of the triad acts as a base to assist the deprotonation of the sulfhydryl group in Cys through the residue His.[43−45] However, mutants H76A and D91A of SmzB still maintained activity similar to that of the wild type of enzyme (Figure 4c). Protein MS also revealed that the mutation of these two amino acid residues had no effect on the acylation of Cys (Figure S37). The mutagenesis results suggested that a different catalytic mechanism is applied by SmzB to achieve the fatty acylation on Cys, which is completely different from the indispensable Cys-His-Asp catalytic triad mechanism in arylamine *N*-acetyltransferases.[43−46]

Site-directed mutagenesis assays showed that mutants Y26A and Y93A completely lost their catalytic activity (Figure 4c), and protein MS revealed that the Cys49 of these two mutants could be still successfully acylated (Figure S37). These facts indicated that the two residues play an essential role in the latter catalytic process involving C−C bond formation between the C-4 of AIR and the C-1 of the fatty acyl linked to Cys49. In the SmzB-AIR docking analysis, residues Tyr26 and Tyr93 residues showed close distances (3.1 and 3.0 Å) to the NH_2 group of AIR (Figure 4b). These interactions suggested a possible proton/electron transfer network of Tyr26, Tyr93, and the NH_2 group of AIR (Figure 4d), which can increase the electron density on the N-atom of NH_2 and further activate the reactivity of C-4 in AIR by the conjugation effect of 5-aminoimidazole ring. The activation can lead to the nucleophilic attack of the C-4 on the carbonyl of the thioester of the fatty acid and thus results in the formation of C−C bonds. When either Tyr26 or Tyr93 residue is mutated, the electron/proton transfer network between AIR and SmzB is disrupted, thus losing the required reactivity of C-4 for FCA reaction. As a result, the catalytic activity of SmzB is lost.

Based on the above analysis, the catalytic mechanism of SmzB is proposed as follows (Figure 4d). The sulfhydryl of SmzB is deprotonated and leads to the nucleophilic attack on the fatty acyl carbon of holo-SmzF, resulting in the formation of an anionic tetrahedral intermediate. Then with the release of holo-SmzF, the intermediate collapses to form the thioester intermediate, fatty acyl-Cys49-SmzB. Next, the substrate AIR is activated by SmzB, causing a nucleophilic addition to form a C−C bond between C-4 in AIR and C-1 of the fatty acid thioesters and thus to generate a protonated imine intermediate connected to SmzB. Subsequently, the C−S bond cleavage occurs with the deprotonation of C-4 in the imine unit and the protonation of the thioether moiety, producing the final products AAIA-1-ribotides. In addition, the oxyanion intermediate was hypothesized to be stabilized by an oxyanion hole probably formed by hydrogen bonds from the polar side chains of Tyr93 and Ser48 and the backbone NH group of Ala50 around Cys49.

As a newly discovered acyltransferase that catalyzes FCA reaction, we also conducted phylogenetic analysis of SmzB. Acyltransferases constitute a very large family that plays a vital role in the biosynthesis of numerous secondary metabolites, protein modification, and other life processes.[47] Here we selected some protein sequences of acyltransferases from UniprotKB, combined with SmzB-like proteins, the PhlCs (a part of ATases), *O*-acyltransferases, serine carboxy peptidases, arylamine *N*-acetyltransferases, palmitoyl transferases (*S*-acyltransferases), and tryptamine *N*-acetyltransferases for phylogenetic analysis.[8,9,41,42,48−54] Results revealed that SmzB and its homologous enzymes were clustered into a new clade, distinct from other acyltransferases, thereby suggesting their involvement in a unique type of acyltransferase function (Figure 5). The ubiquitous distribution of SmzB-like enzymes

https://doi.org/10.1021/jacs.3c09522
J. Am. Chem. Soc. XXXX, XXX, XXX−XXX

in microorganisms implies a pivotal function in the biosynthesis of natural products by FCA reaction.

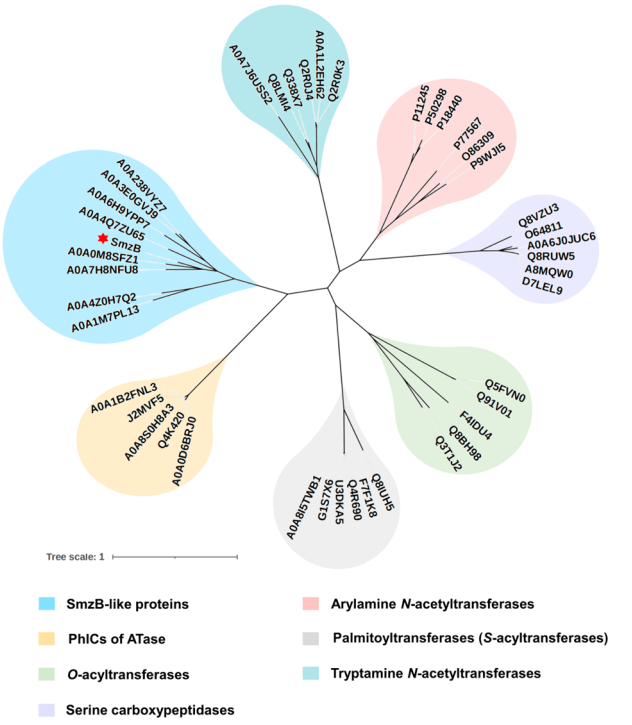

Figure 5. Phylogenetic analysis of SmzBs, PhlCs, arylamine *N*-acetyltransferases, and other acyltransferases. The names of proteins are represented by accessions in UniprotKB.

CONCLUSIONS

In summary, the biosynthesis of AAIAs has been fully elucidated in this study. Four key enzymes SmzB, -C, -E, and -F have been proved to be responsible for the biosynthesis of AAIAs. The unique acyltransferase SmzB has been characterized as a new FCase that catalyzes the FCA reaction between ortho-aromatic carbon of amino in AIR and carbonyl carbon of fatty acid thioesters. Structural simulation and molecular modeling of SmzB, together with site-directed mutagenesis, provide new insights into the catalytic mechanism of the enzymatic FCA reaction. The successful exploration of the broadness of fatty acid substrates for enzymatic synthesis of AAIAs has greatly contributed to expanding the structural diversity of such alkaloids. This breakthrough in enzymatic synthesis of AAIAs represents an important advancement in the field of alkaloid research and may lead to further opportunities for structural exploration.

ASSOCIATED CONTENT

Supporting Information

The Supporting Information is available free of charge at https://pubs.acs.org/doi/10.1021/jacs.3c09522.

Materials, general experimental procedures, experimental details, supplementary tables, supplementary figures, and NMR spectra (PDF)

Accession Codes

The sequence of putative *smz* biosynthetic gene cluster can be found in the GenBank database under accession number OR086932.

AUTHOR INFORMATION

Corresponding Authors

Lei Du − *State Key Laboratory of Microbial Technology, Shandong University, Qingdao 266237, China;* orcid.org/0000-0003-2245-7100; Email: lei.du@sdu.edu.cn

Weiming Zhu − *Key Laboratory of Marine Drugs, Ministry of Education of China, School of Medicine and Pharmacy, Ocean University of China, Qingdao 266003, China; Laboratory for Marine Drugs and Bioproducts, Laoshan Laboratory, Qingdao 266237, China;* orcid.org/0000-0002-7591-3264; Email: weimingzhu@ouc.edu.cn

Authors

Yuwei Xia − *Key Laboratory of Marine Drugs, Ministry of Education of China, School of Medicine and Pharmacy, Ocean University of China, Qingdao 266003, China*

Guoliang Zhu − *Key Laboratory of Marine Drugs, Ministry of Education of China, School of Medicine and Pharmacy, Ocean University of China, Qingdao 266003, China;* Present Address: State Key Laboratory of Bioreactor Engineering, East China University of Science and Technology, Shanghai 200237, China

Xingwang Zhang − *State Key Laboratory of Microbial Technology, Shandong University, Qingdao 266237, China;* orcid.org/0000-0003-1346-1183

Shengying Li − *State Key Laboratory of Microbial Technology, Shandong University, Qingdao 266237, China;* orcid.org/0000-0002-5244-870X

Complete contact information is available at: https://pubs.acs.org/10.1021/jacs.3c09522

Author Contributions

[⊥]Y. Xia, G. Zhu, and X. Zhang contributed equally to this paper.

Notes

The authors declare no competing financial interest.

ACKNOWLEDGMENTS

This research was supported by National Key Research and Development Program of China (Grants 2022YFC2804100 and 2021YFA0911500), National Natural Science Foundation of China (Grants U1906213 and 32170088), and Shandong Provincial Natural Science Foundation (Grant ZR2020ZD23). The authors acknowledge Shandong University Core Facilities for Life and Environmental Sciences for their help in the protein ESI-Q-TOF-MS analysis. The authors acknowledge the ZCloud platform (https://cloud.zelixir.com, Shanghai ZELIX-IR BIOTECH) for the help in part of the computations of multiple biomolecule structure modeling, simulation, and prediction algorithms.

REFERENCES

(1) Sartori, G.; Maggi, R. *Advances in Friedel-Crafts Acylation Reactions*; CRC Press: Boca Raton, FL, USA, 2010; pp 9−28.

(2) Kürti, L.; Czakó, B. *Strategic Applications of Named Reactions in Organic Synthesis*; Elsevier Academic Press: Burlington, MA, USA, 2005; pp 176−177.

(3) Effenberger, F.; Epple, G. Catalytic Friedel-Crafts acylation of aromatic compounds. *Angew. Chem., Int. Ed.* **1972**, *11*, 300−301.

(4) Vollhardt, K. P. C.; Schore, N. E. *Organic Chemistry: Structure and Function*, 7th ed.; W. H. Freeman Press: New York, USA, 2014; pp 680−689.

(5) Xing, Q.; Pei, W.; Xu, R.; Pei, J. *Basic Organic Chemistry*, 3rd ed.; Higher Education Press: Beijing, China, 2005; pp 482−483.
(6) Leveson-Gower, R. B.; Roelfes, G. Biocatalytic Friedel-Crafts reactions. *ChemCatChem* **2022**, *14*, No. e202200636.
(7) Kumar, V.; Turnbull, W. B.; Kumar, A. Review on recent developments in biocatalysts for Friedel−Crafts reactions. *ACS Catal.* **2022**, *12*, 10742−10763.
(8) Hayashi, A.; Saitou, H.; Mori, T.; Matano, I.; Sugisaki, H.; Maruyama, K. Molecular and catalytic properties of monoacetylphloroglucinol acetyltransferase from *Pseudomonas* sp. YGJ3. *Biosci. Biotechnol. Biochem.* **2012**, *76*, 559−566.
(9) Bangera, M. G.; Thomashow, L. S. Identification and characterization of a gene cluster for synthesis of the polyketide antibiotic 2,4-diacetylphloroglucinol from *Pseudomonas fluorescens* Q2-87. *J. Bacteriol.* **1999**, *181*, 3155−3163.
(10) Schmidt, N. G.; Pavkov-Keller, T.; Richter, N.; Wiltschi, B.; Gruber, K.; Kroutil, W. Biocatalytic Friedel-Crafts acylation and Fries reaction. *Angew. Chem., Int. Ed. Engl.* **2017**, *56*, 7615−7619.
(11) Schmidt, N. G.; Kroutil, W. Acyl donors and additives for the biocatalytic Friedel−Crafts acylation. *Eur. J. Org. Chem.* **2017**, *2017*, 5865−5871.
(12) Żądło-Dobrowolska, A.; Schmidt, N. G.; Kroutil, W. Thioesters as acyl donors in biocatalytic Friedel-Crafts-type acylation catalyzed by acyltransferase from *Pseudomonas Protegens*. *ChemCatChem.* **2019**, *11*, 1064−1068.
(13) Pavkov-Keller, T.; Schmidt, N. G.; Żądło-Dobrowolska, A.; Kroutil, W.; Gruber, K. Structure and catalytic mechanism of a bacterial Friedel-Crafts acylase. *Chembiochem* **2019**, *20*, 88−95.
(14) Sheng, X.; Kazemi, M.; Żądło-Dobrowolska, A.; Kroutil, W.; Himo, F. Mechanism of biocatalytic Friedel-Crafts acylation by acyltransferase from *Pseudomonas protegens*. *ACS Catal.* **2020**, *10*, 570−577.
(15) Żądło-Dobrowolska, A.; Hammerer, L.; Pavkov-Keller, T.; Gruber, K.; Kroutil, W. Rational engineered C-acyltransferase transforms sterically demanding acyl donors. *ACS Catal.* **2020**, *10*, 1094−1101.
(16) Leutou, A. S.; Yang, I.; Kang, H.; Seo, E. K.; Nam, S. J.; Fenical, W. Nocarimidazoles A and B from a marine-derived actinomycete of the genus *Nocardiopsis*. *J. Nat. Prod.* **2015**, *78*, 2846−2849.
(17) Karim, M. R. U.; Harunari, E.; Sharma, A. R.; Oku, N.; Akasaka, K.; Urabe, D.; Sibero, M. T.; Igarashi, Y. Nocarimidazoles C and D, antimicrobial alkanoylimidazoles from a coral-derived actinomycete *Kocuria* sp.: application of $^{1}J_{C,H}$ coupling constants for the unequivocal determination of substituted imidazoles and stereochemical diversity of anteisoalkyl chains in microbial metabolites. *Beilstein J. Org. Chem.* **2020**, *16*, 2719−2727.
(18) Blin, K.; Shaw, S.; Steinke, K.; Villebro, R.; Ziemert, N.; Lee, S. Y.; Medema, M. H.; Weber, T. AntiSMASH 5.0: updates to the secondary metabolite genome mining pipeline. *Nucleic Acids Res.* **2019**, *47*, W81−W87.
(19) Schrimsher, J. L.; Schendel, F. J.; Stubbe, J.; Smith, J. M. Purification and characterization of aminoimidazole ribonucleotide synthetase from *Escherichia coli*. *Biochemistry* **1986**, *25*, 4366−4371.
(20) Cheng, Y. S.; Shen, Y.; Rudolph, J.; Stern, M.; Stubbe, J.; Flannigan, K. A.; Smith, J. M. Glycinamide ribonucleotide synthetase from *Escherichia coli*: cloning, overproduction, sequencing, isolation, and characterization. *Biochemistry* **1990**, *29*, 218−227.
(21) Fujiwara, K.; Okamura-Ikeda, K.; Ohmura, Y.; Motokawa, Y. Mechanism of the glycine cleavage reaction: retention of C-2 hydrogens of glycine on the intermediate attached to H-protein and evidence for the inability of serine hydroxymethyltransferase to catalyze the glycine decarboxylation. *Arch. Biochem. Biophys.* **1986**, *251*, 121−127.
(22) Edwards, P.; Nelsen, J. S.; Metz, J. G.; Dehesh, K. Cloning of the fabF gene in an expression vector and in vitro characterization of recombinant fabF and fabB encoded enzymes from *Escherichia coli*. *FEBS Lett.* **1997**, *402*, 62−66.
(23) Wakil, S. J. Fatty acid synthase, a proficient multifunctional enzyme. *Biochemistry* **1989**, *28*, 4523−4530.
(24) Venugopal, A.; Bryk, R.; Shi, S.; Rhee, K.; Rath, P.; Schnappinger, D.; Ehrt, S.; Nathan, C. Virulence of *Mycobacterium tuberculosis* depends on lipoamide dehydrogenase, a member of three multienzyme complexes. *Cell Host Microbe* **2011**, *9*, 21−31.
(25) Wiker, F.; Konnerth, M.; Helmle, I.; Kulik, A.; Kaysser, L.; Gross, H.; Gust, B. Identification of novel α-pyrones from *Conexibacter woesei* serving as sulfate shuttles. *ACS Chem. Biol.* **2019**, *14*, 1972−1980.
(26) Harig, T.; Schlawis, C.; Ziesche, L.; Pohlner, M.; Engelen, B.; Schulz, S. Nitrogen-containing volatiles from marine *Salinispora pacifica* and *Roseobacter*-group bacteria. *J. Nat. Prod.* **2017**, *80*, 3289−3295.
(27) Ma, J.; Zhang, P.; Zhang, Z.; Zha, M.; Xu, H.; Zhao, G.; Ding, J. Molecular basis of the substrate specificity and the catalytic mechanism of citramalate synthase from *Leptospira interrogans*. *Biochem. J.* **2008**, *415*, 45−56.
(28) Cheng, Y. S.; Shen, Y.; Rudolph, J.; Stern, M.; Stubbe, J.; Flannigan, K. A.; Smith, J. M. Glycinamide ribonucleotide synthetase from *Escherichia coli*: cloning, overproduction, sequencing, isolation, and characterization. *Biochemistry* **1990**, *29*, 218−227.
(29) Inglese, J.; Johnson, D. L.; Shiau, A.; Smith, J. M.; Benkovic, S. J. Subcloning, characterization, and affinity labeling of *Escherichia coli* glycinamide ribonucleotide transformylase. *Biochemistry* **1990**, *29*, 1436−1443.
(30) Hoskins, A. A.; Anand, R.; Ealick, S. E.; Stubbe, J. The formylglycinamide ribonucleotide amidotransferase complex from *Bacillus subtilis*: metabolite-mediated complex formation. *Biochemistry* **2004**, *43*, 10314−10327.
(31) Wang, W.; Li, X.; Wang, J.; Xiang, S.; Feng, X.; Yang, K. An engineered strong promoter for streptomycetes. *Appl. Environ. Microbiol.* **2013**, *79*, 4484−4492.
(32) Sánchez, C.; Du, L.; Edwards, D. J.; Toney, M. D.; Shen, B. Cloning and characterization of a phosphopantetheinyl transferase from *Streptomyces verticillus* ATCC15003, the producer of the hybrid peptide-polyketide antitumor drug bleomycin. *Chem. Biol.* **2001**, *8*, 725−738.
(33) Quadri, L. E.; Weinreb, P. H.; Lei, M.; Nakano, M. M.; Zuber, P.; Walsh, C. T. Characterization of Sfp, a *Bacillus subtilis* phosphopantetheinyl transferase for peptidyl carrier protein domains in peptide synthetases. *Biochemistry* **1998**, *37*, 1585−1595.
(34) Proudfoot, M.; Kuznetsova, E.; Brown, G.; Rao, N. N.; Kitagawa, M.; Mori, H.; Savchenko, A.; Yakunin, A. F. General enzymatic screens identify three new nucleotidases in *Escherichia coli*. Biochemical characterization of SurE. *YfbR, and YjjG. J. Biol. Chem.* **2004**, *279*, 54687−54694.
(35) Guddat, L. W.; Vos, S.; Martin, J. L.; Keough, D. T.; de Jersey, J. Crystal structures of free, IMP-, and GMP-bound *Escherichia coli* hypoxanthine phosphoribosyltransferase. *Protein Sci.* **2002**, *11*, 1626−1638.
(36) Leung, H. B.; Schramm, V. L. Adenylate degradation in *Escherichia coli*. The role of AMP nucleosidase and properties of the purified enzyme. *J. Biol. Chem.* **1980**, *255*, 10867−10874.
(37) Aono, R.; Sato, T.; Yano, A.; Yoshida, S.; Nishitani, Y.; Miki, K.; Imanaka, T.; Atomi, H. Enzymatic characterization of AMP phosphorylase and ribose-1,5-bisphosphate isomerase functioning in an archaeal AMP metabolic pathway. *J. Bacteriol.* **2012**, *194*, 6847−6855.
(38) Karim, M. R. U.; Harunari, E.; Oku, N.; Akasaka, K.; Igarashi, Y. Bulbimidazoles A−C, antimicrobial and cytotoxic alkanoyl imidazoles from a marine gammaproteobacterium *Microbulbifer* species. *J. Nat. Prod.* **2020**, *83*, 1295−1299.
(39) Sun, X.; Wang, G.; Xiao, H.; Jiang, J.; Xiao, D.; Xing, B.; Li, A.; Zhang, Y.; Sun, K.; Xu, Y.; Guo, L.; Yang, D.; Ma, M. Strepimidazoles A−G from the plant endophytic *Streptomyces* sp. PKU-EA00015 with inhibitory activities against a plant pathogenic fungus. *J. Nat. Prod.* **2020**, *83*, 2246−2254.
(40) Jumper, J.; Evans, R.; Pritzel, A.; Green, T.; Figurnov, M.; Ronneberger, O.; Tunyasuvunakool, K.; Bates, R.; Žídek, A.; Potapenko, A.; Bridgland, A.; Meyer, C.; Kohl, S. A. A.; Ballard, A.

https://doi.org/10.1021/jacs.3c09522
J. Am. Chem. Soc. XXXX, XXX, XXX−XXX

J.; Cowie, A.; Romera-Paredes, B.; Nikolov, S.; Jain, R.; Adler, J.; Back, T.; Petersen, S.; Reiman, D.; Clancy, E.; Zielinski, M.; Steinegger, M.; Pacholska, M.; Berghammer, T.; Bodenstein, S.; Silver, D.; Vinyals, O.; Senior, A. W.; Kavukcuoglu, K.; Kohli, P.; Hassabis, D. Highly accurate protein structure prediction with AlphaFold. *Nature* **2021**, *596*, 583−589.
(41) Wu, H.; Dombrovsky, L.; Tempel, W.; Martin, F.; Loppnau, P.; Goodfellow, G. H.; Grant, D. M.; Plotnikov, A. N. Structural basis of substrate-binding specificity of human arylamine *N*-acetyltransferases. *J. Biol. Chem.* **2007**, *282*, 30189−30197.
(42) Sinclair, J. C.; Sandy, J.; Delgoda, R.; Sim, E.; Noble, M. E. Structure of arylamine *N*-acetyltransferase reveals a catalytic triad. *Nat. Struct. Biol.* **2000**, *7*, 560−564.
(43) Kubiak, X.; Li de la Sierra-Gallay, I.; Chaffotte, A. F.; Pluvinage, B.; Weber, P.; Haouz, A.; Dupret, J. M.; Rodrigues-Lima, F. Structural and biochemical characterization of an active arylamine *N*-acetyltransferase possessing a non-canonical Cys-His-Glu catalytic triad. *J. Biol. Chem.* **2013**, *288*, 22493−22505.
(44) Sikora, A. L.; Frankel, B. A.; Blanchard, J. S. Kinetic and chemical mechanism of arylamine *N*-acetyltransferase from *Mycobacterium tuberculosis*. *Biochemistry* **2008**, *47*, 10781−10789.
(45) Wang, H.; Vath, G. M.; Gleason, K. J.; Hanna, P. E.; Wagner, C. R. Probing the mechanism of hamster arylamine *N*-acetyltransferase 2 acetylation by active site modification, site-directed mutagenesis, and pre-steady state and steady state kinetic studies. *Biochemistry* **2004**, *43*, 8234−8246.
(46) Sandy, J.; Mushtaq, A.; Holton, S. J.; Schartau, P.; Noble, M. E.; Sim, E. Investigation of the catalytic triad of arylamine *N*-acetyltransferases: essential residues required for acetyl transfer to arylamines. *Biochem. J.* **2005**, *390*, 115−123.
(47) Röttig, A.; Steinbüchel, A. Acyltransferases in bacteria. *Microbiol. Mol. Biol. Rev.* **2013**, *77*, 277−321.
(48) Greaves, J.; Munro, K. R.; Davidson, S. C.; Riviere, M.; Wojno, J.; Smith, T. K.; Tomkinson, N. C.; Chamberlain, L. H. Molecular basis of fatty acid selectivity in the zDHHC family of *S*-acyltransferases revealed by click chemistry. *Proc. Natl. Acad. Sci. U. S. A.* **2017**, *114*, E1365−E1374.
(49) Lemonidis, K.; Gorleku, O. A.; Sanchez-Perez, M. C.; Grefen, C.; Chamberlain, L. H. The Golgi *S*-acylation machinery comprises zDHHC enzymes with major differences in substrate affinity and S-acylation activity. *Mol. Biol. Cell* **2014**, *25*, 3870−3883.
(50) Shirley, A. M.; Chapple, C. Biochemical characterization of sinapoylglucose:choline sinapoyltransferase, a serine carboxypeptidase-like protein that functions as an acyltransferase in plant secondary metabolism. *J. Biol. Chem.* **2003**, *278*, 19870−19877.
(51) Fraser, C. M.; Thompson, M. G.; Shirley, A. M.; Ralph, J.; Schoenherr, J. A.; Sinlapadech, T.; Hall, M. C.; Chapple, C. Related arabidopsis serine carboxypeptidase-like sinapoylglucose acyltransferases display distinct but overlapping substrate specificities. *Plant Physiol.* **2007**, *144*, 1986−1999.
(52) Peng, M.; Gao, Y.; Chen, W.; Wang, W.; Shen, S.; Shi, J.; Wang, C.; Zhang, Y.; Zou, L.; Wang, S.; Wan, J.; Liu, X.; Gong, L.; Luo, J. Evolutionarily distinct BAHD *N*-acyltransferases are responsible for natural variation of aromatic amine conjugates in rice. *Plant Cell* **2016**, *28*, 1533−1550.
(53) Hishikawa, D.; Shindou, H.; Kobayashi, S.; Nakanishi, H.; Taguchi, R.; Shimizu, T. Discovery of a lysophospholipid acyltransferase family essential for membrane asymmetry and diversity. *Proc. Natl. Acad. Sci. U. S. A.* **2008**, *105*, 2830−2835.
(54) Hashidate-Yoshida, T.; Harayama, T.; Hishikawa, D.; Morimoto, R.; Hamano, F.; Tokuoka, S. M.; Eto, M.; Tamura-Nakano, M.; Yanobu-Takanashi, R.; Mukumoto, Y.; Kiyonari, H.; Okamura, T.; Kita, Y.; Shindou, H.; Shimizu, T. Fatty acid remodeling by LPCAT3 enriches arachidonate in phospholipid membranes and regulates triglyceride transport. *eLife* **2015**, *4*, No. e06328.

https://doi.org/10.1021/jacs.3c09522
J. Am. Chem. Soc. XXXX, XXX, XXX−XXX